SCIENCE CHINA
Life Sciences

•RESEARCH PAPER•

February 2020 Vol.63 No.2: 239–250
https://doi.org/10.1007/s11427-019-9532-0

# *Arabidopsis* AIP1-1 regulates the organization of apical actin filaments by promoting their turnover in pollen tubes

Min Diao[1,2,4], Xin Li[1,3] & Shanjin Huang[2*]

[1]*Institute of Botany, Chinese Academy of Sciences, Beijing 100093, China;*
[2]*Center for Plant Biology, School of Life Sciences, Tsinghua University, Beijing 100084, China;*
[3]*University of Chinese Academy of Sciences, Beijing 100049, China;*
[4]*iHuman Institute, Shanghai Tech University, Shanghai 201210, China*

Received February 28, 2019; accepted April 2, 2019; published online June 25, 2019

Apical actin filaments are highly dynamic structures that are crucial for rapid pollen tube growth, but the mechanisms regulating their dynamics and spatial organization remain incompletely understood. We here identify that AtAIP1-1 is important for regulating the turnover and organization of apical actin filaments in pollen tubes. AtAIP1-1 is distributed uniformly in the pollen tube and loss of function of *AtAIP1-1* affects the organization of the actin cytoskeleton in the pollen tube. Specifically, actin filaments became disorganized within the apical region of *aip1-1* pollen tubes. Consistent with the role of apical actin filaments in spatially restricting vesicles in pollen tubes, the apical region occupied by vesicles becomes enlarged in *aip1-1* pollen tubes compared to WT. Using ADF1 as a representative actin-depolymerizing factor, we demonstrate that AtAIP1-1 enhances ADF1-mediated actin depolymerization and filament severing *in vitro*, although AtAIP1-1 alone does not have an obvious effect on actin assembly and disassembly. The dynamics of apical actin filaments are reduced in *aip1-1* pollen tubes compared to WT. Our study suggests that AtAIP1-1 works together with ADF to act as a module in regulating the dynamics of apical actin filaments to facilitate the construction of the unique "apical actin structure" in the pollen tube.

**pollen tube, apical actin structure, actin dynamics, actin turnover, ADF, AIP1**

**Citation:** Diao, M., Li, X., and Huang, S. (2020). *Arabidopsis* AIP1-1 regulates the organization of apical actin filaments by promoting their turnover in pollen tubes. Sci China Life Sci 63, 239–250. https://doi.org/10.1007/s11427-019-9532-0

## INTRODUCTION

Pollen tube growth depends on a dynamically remodeled actin cytoskeleton, which is organized into distinct structures in different regions of the pollen tube (Chen et al., 2009; Cheung and Wu, 2008; Fu, 2015; Qu et al., 2015; Ren and Xiang, 2007; Staiger et al., 2010). Actin filaments within the apical region are presumably more directly involved in the regulation of pollen tube growth and turning by controlling vesicle trafficking as well as exocytic and endocytic events to drive membrane expansion and cell wall synthesis. In support of this notion, treatment with a low dosage of the actin depolymerizing agent latrunculin B (LatB) quite specifically alters the dynamics of apical actin filaments, which leads to arrested pollen tube growth, but has no obvious effect on shank-localized longitudinal actin cables and cytoplasmic streaming (Gibbon et al., 1999; Vidali et al., 2001). Previous observations showed that actin filaments are mainly generated from the plasma membrane (PM) within the growth domain of the pollen tube (Cheung et al., 2010; Lan et al., 2018; Liu et al., 2015; Qu et al., 2013; Zhang et al., 2016), and these actin filaments are arrayed into the distinct "apical actin structure" in the pollen tube (Qu et al., 2017). However, we still have an incomplete understanding of the mechanisms that generate an apical actin structure that is properly organized yet can still be dynamically remodeled to

*Corresponding author (email: sjhuang@tsinghua.edu.cn)

support rapid polarized pollen tube growth.

As the central regulator of actin turnover, actin-depolymerizing factor (ADF) has been implicated in the regulation of actin dynamics in pollen cells (Bou Daher et al., 2011; Chen et al., 2002; Daher and Geitmann, 2012; Jiang et al., 2017; Smertenko et al., 2001; Zheng et al., 2013; Zhu et al., 2017). In particular, it has been confirmed that ADF has a role in promoting the turnover and ordering of apical actin filaments as well as the construction of the apical actin structure in pollen tubes (Jiang et al., 2017). Understanding how the activity of ADF is regulated will provide insights into the regulation of the apical actin structure in pollen tubes. Actin-interacting protein 1 (AIP1) was originally identified as an actin-interacting protein in yeast (Amberg et al., 1995), and was subsequently shown to interact with cofilin and enhance cofilin-mediated actin depolymerization *in vitro* (Rodal et al., 1999). The ability of plant AIP1 proteins to enhance ADF-mediated actin depolymerization has been confirmed *in vitro* (Allwood et al., 2002; Shi et al., 2013) and *in vivo* (Augustine et al., 2011; Shi et al., 2013). In addition, AIP1 has been implicated in the regulation of plant growth and development (Ketelaar et al., 2004; Kiefer et al., 2015). Although AIP1 is a likely candidate player in regulating the unique apical actin structure in the pollen tube, it remains to be documented how exactly AIP1 regulates the dynamics and organization of apical actin filaments and the construction of the apical actin structure in pollen tubes.

Here, we characterized the function and mechanism of action of *Arabidopsis* AIP1-1 (AtAIP1-1) in regulating actin dynamics within the apical region of pollen tubes using a combination of state-of-the-art *in vitro* biochemical assays and live-cell imaging technology. We found that loss of function of *AtAIP1-1* induces disorganization of apical actin filaments, which impairs the formation of the apical actin structure and consequently alters the pattern of vesicle accumulation in pollen tubes. Live-cell imaging of the dynamics of actin filaments showed that actin filament severing and monomer dissociation events are reduced in *aip1-1* pollen tubes. Consistent with these findings, AtAIP1-1 enhances ADF1-mediated actin filament severing and monomer dissociation *in vitro*. Our study suggests that AtAIP1-1 acts in concert with ADF in regulating the turnover of actin filaments within the growth domain of pollen tubes and facilitates the construction of the apical actin structure.

## RESULTS

### Loss of function of *Arabidopsis AIP1-1* impairs pollen germination and pollen tube growth

Previous study showed that there are two *AIP1*-like genes in the *Arabidopsis* genome, designated as *AtAIP1-1* and *AtAIP1-2* (Allwood et al., 2002). *AtAIP1-1* is expressed specifically in pollen (https://genevestigator.com/gv/). To analyze the function of *AtAIP1-1* in regulating actin dynamics in pollen tubes, we obtained a mutant line with T-DNA inserted in the second exon of the gene (Figure 1A). We found that it is a knockout mutant since full-length *AtAIP1-1* transcripts are absent (Figure 1B). We next performed *in vitro* germination experiments to determine the effect of loss of function of *AtAIP1-1* on pollen germination and pollen tube growth. The pollen germination percentages and pollen tube growth rates are reduced significantly in *aip1-1* mutants compared to WT (Figure 1C–F). To complement *aip1-1* mutant, we generated an AtAIP1-1-EGFP fusion construct driven by the native *AtAIP1-1* promoter. After transforming the fusion construct into the *aip1-1* mutant, we found that the level of *AtAIP1-1* transcripts is restored (Figure S1A in Supporting Information) and the pollen germination defects are rescued (Figure S1B and C in Supporting Information), which suggests that the phenotype in *aip1-1* mutants is indeed caused by the loss of function of *AtAIP1-1*. Thus, our results suggest that loss of function of *AtAIP1-1* inhibits pollen germination and pollen tube growth.

### Loss of function of *AtAIP1-1* induces disorganization of apical actin filaments and impairs the formation of the apical actin structure at the pollen tube tip

We next examined the organization of actin filaments in pollen tubes by staining with Alexa-488-phalloidin as described previously (Zhang et al., 2010a). The fluorescence intensity of actin filaments appeared to be higher in the middle region of *aip1-1* pollen tubes than that of WT tubes (Figure 2A–C). Statistical analysis of the results showed that the average fluorescence intensity of shank-localized actin filaments in *aip1-1* pollen tubes is significantly higher than that in WT pollen tubes (Figure 2D). In line with this finding, we found that the rate of actin turnover is reduced in *aip1-1* pollen grains, which is evidenced by the insensitivity of the actin cytoskeleton to LatB treatment (Figure S1C and D in Supporting Information). Specifically, after treatment with the actin polymerization inhibitor LatB (150 nmol $L^{-1}$), actin filaments became fragmented in WT pollen grains, whereas actin filaments are intact and form heavy bundles in *aip1-1* pollen grains (Figure S1C and D in Supporting Information). In addition, the sensitivity of the actin cytoskeleton to treatment with LatB is restored in pollen grains derived from the *AtAIP1-1* complementation line (Figure S1D in Supporting Information), which suggests that the actin turnover defect in *aip1-1* pollen grains is indeed caused by the loss of function of *AtAIP1-1*. There was no significant difference in the fluorescence intensity of actin filaments within the apical and subapical regions of *aip1-1* pollen tubes when compared to those in WT pollen tubes (Figure 2E). However, the actin

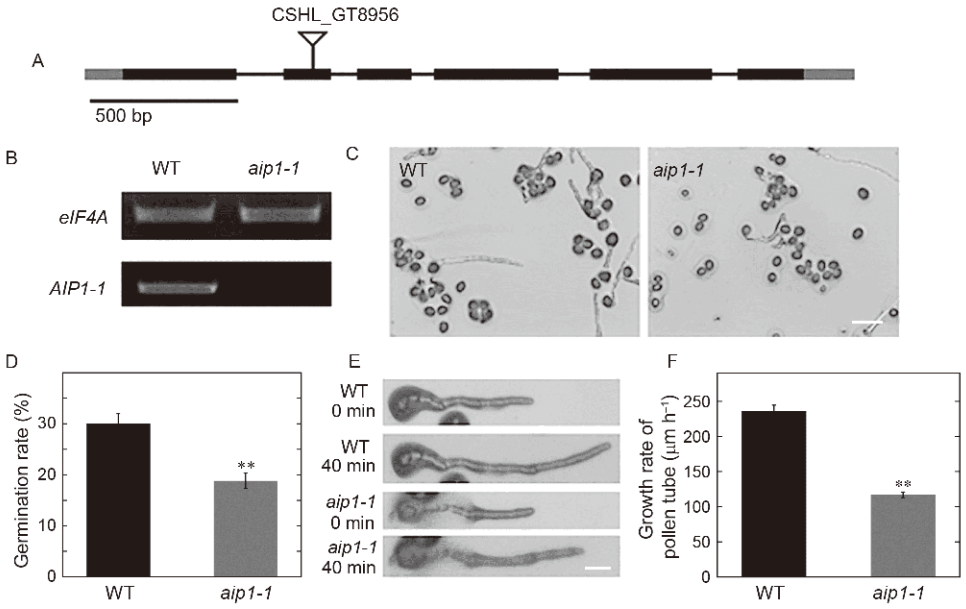


**Figure 1** Loss of function of *AtAIP1-1* impairs pollen germination and pollen tube growth. A, Physical structure of *AtAIP1-1*. Black boxes and lines indicate exons and introns, respectively. Gray boxes indicate 5′-UTR and 3′-UTR. The T-DNA insertion site in the second exon is also shown. B, RT-PCR analysis of *AtAIP1-1* transcripts. *eIF4A* was amplified as the control. C, Micrographs of pollen germinated on germination medium for 1.5 h. Scale bar, 100 μm. D, Quantification of pollen germination percentage. Data are presented as mean±SE. **, $P<0.01$ by $\chi^2$ test. E, Micrographs of pollen tubes. Representative pollen tubes at two time points are presented. Scale bar, 20 μm. F, Quantification of pollen tube growth rates. Data are presented as mean±SE. **, $P<0.01$ by Student's *t*-test.

filaments appeared more disorganized in *aip1-1* pollen tubes compared to WT (Figure 2A), which was supported by measurements showing that the angles formed between the apical actin filaments and the growth axis of pollen tubes were substantially increased in *aip1-1* pollen tubes compared to WT pollen tubes (Figure 2F). Interestingly, we found that the region with less actin filaments extends a lot further from the pollen tube tip toward the tube base in *aip1-1* pollen tubes compared to WT pollen tubes (Figure 2A). Nonetheless, these data together suggest that loss of function of *AtAIP1-1* increases the amount of shank-localized actin filaments and causes disorganization of actin filaments within the apical and subapical regions of pollen tubes.

### Loss of function of *AtAIP1-1* affects the apical accumulation pattern and tip-directed movement of vesicles in pollen tubes

Actin filaments within the apical and subapical regions of pollen tubes are involved in regulating the transport and accumulation of vesicles. Therefore, we examined whether the vesicle accumulation pattern and tip-directed trafficking were altered in *aip1-1* pollen tubes. We used YFP-RabA4b to decorate transport vesicles as described previously (Zhang et al., 2010b). The results showed that the accumulated vesicles in the apical region of WT pollen tubes exhibited an inverted "V" shape (Figure 3A). However, the region of vesicle accumulation was enlarged in *aip1-1* pollen tubes compared to WT pollen tubes (Figure 3A), and this was supported by visualizing the YFP-RabA4b-decorated vesicles in transverse sections of pollen tubes (Figure 3B). Further observations revealed that the enlargement of the vesicle accumulation region was maintained during pollen tube growth (Figure 3C). The vesicle accumulation data are consistent with the above data showing that the region with less actin filaments became enlarged in *aip1-1* pollen tubes (Figure 2A). These data support the notion that apical actin filaments act as the physical barrier to spatially restrict vesicles at the tip of pollen tubes. To quantify the tip-directed transportation of vesicles in WT and *aip1-1* pollen tubes, we performed fluorescence recovery after photobleaching (FRAP) experiments for both WT and *aip1-1* pollen tubes (Figure S2A in Supporting Information) and found that the rate of FRAP is substantially reduced in *aip1-1* pollen tubes (Figure S2B in Supporting Information). This suggests that the rate of turnover of vesicles is reduced in *aip1-1* pollen tubes, which implies that the tip-directed movement of vesicles is impaired in *aip1-1* pollen tubes. As the amount of vesicles accumulate at the tip of pollen tubes depends on the relative change in the tipward and backward movement of vesicles, our data imply that the backward movement of vesicles was also impaired in *aip1-1* pollen tubes. Nonetheless, these data together suggest that the tip-directed transportation and accumulation of vesicles are altered in *aip1-1* pollen tubes.

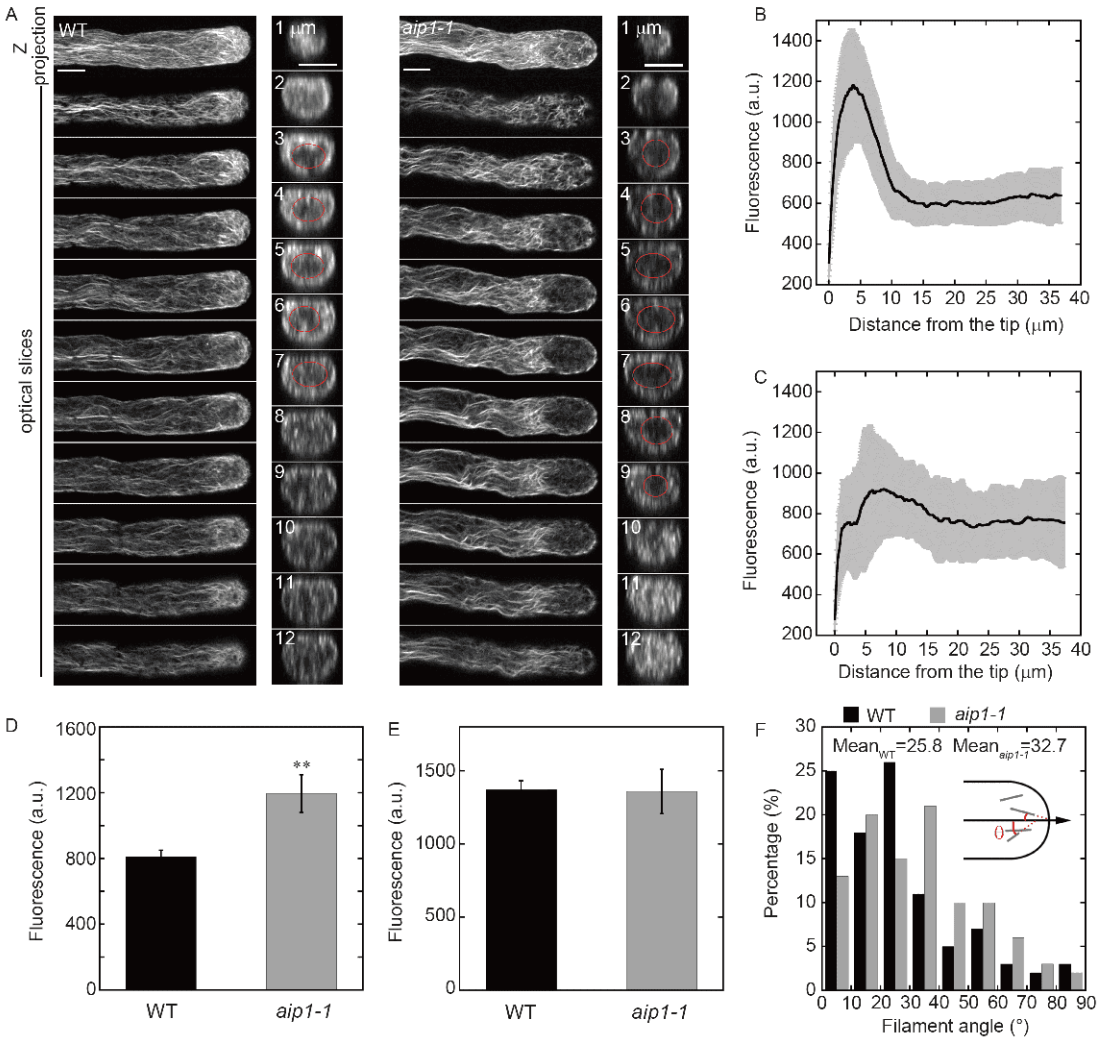


**Figure 2** Membrane-originated actin filaments within the apical region of pollen tubes become lengthened in *aip1-1*. A, Actin filaments in WT (left) and *aip1-1* (right) pollen tubes revealed by staining with Alexa-488 phalloidin. The projection image and optical sections are presented. The right panels are transverse sections; the distances from the tip of the pollen tubes are indicated on the image. Scale bar, 5 μm. B, Plot of the fluorescence intensity of actin staining starting from the tip of WT pollen tubes. Results are presented as mean±SE (the black line is the mean and the shaded region shows the SE). More than 20 pollen tubes were measured. C, Plot of the fluorescence intensity of actin staining starting from the tip of *aip1-1* pollen tubes. Results are presented as mean±SE (the black line is the mean and the shaded region shows the SE). More than 20 pollen tubes were measured. D, Quantification of the average fluorescence intensity of actin filaments within the region that is 10–30 μm from the tip of the pollen tube. Data are presented as mean±SE. More than 20 pollen tubes were measured. **, $P<0.01$ by Student's *t*-test. E, Quantification of the average fluorescence intensity of actin filaments within the region that is 0–10 μm from the tip of pollen tubes. Data are presented as mean±SE. F, Quantification of the angles formed between apical actin filaments and the growth axis of pollen tubes. More than 100 actin filaments were measured from 15 pollen tubes. The inset image shows the schematic diagram describing how we measured the angles formed between actin filaments and the growth axis of pollen tubes. Actin filaments were indicated by green lines, and the growth axis of pollen tube was indicated by a black arrow. θ represents the angle formed between F-actin and the growth axis of the pollen tube.

### AtAIP1-1 is distributed uniformly in the cytoplasm throughout the entire pollen tube

After establishing that AtAIP1-1-EGFP is a functional fusion construct (Figure S1 in Supporting Information), we used it to indicate the intracellular localization of AtAIP1-1 in pollen tubes. We found that although AtAIP1-1 binds to actin filaments *in vitro* (see below), AtAIP1-1-EGFP is distributed quite uniformly within the cytoplasm of the pollen tube and does not form obvious filamentous structures (Figure 4A). Fluorescence intensity measurements showed that the distribution of AtAIP1-1-EGFP is quite uniform within the cytoplasm of the entire pollen tube (Figure 4B). We did not notice any concentration of AtAIP1-1-EGFP at the subapex, which contrasts with a previous study in which the localization of AIP1 in pollen tubes was revealed by immunostaining with an anti-AIP1 antibody (Lovy-Wheeler et al., 2006).

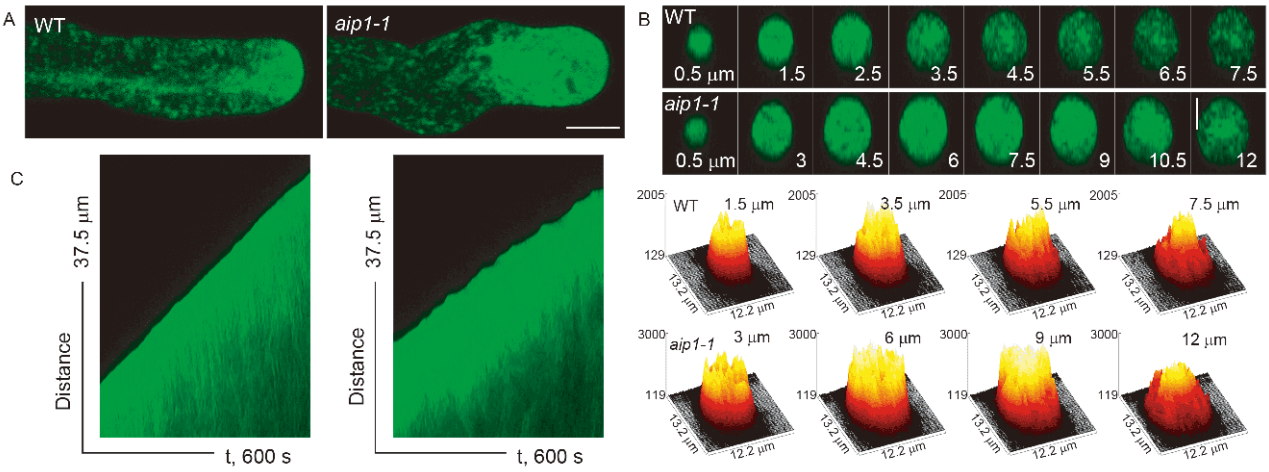


**Figure 3** The regions of apical vesicle accumulation is enlarged in *aip1-1* pollen tubes. A, Images of YFP-RabA4-labeled vesicles in WT and *aip1-1* pollen tubes. Scale bar, 5 μm. B, The upper panel shows transverse sections of WT and *aip1-1* pollen tubes. The distances from the tip of the pollen tubes are shown. Scale bar, 5 μm. The lower panel shows three-dimensional analysis of the distribution of the fluorescence intensity of vesicles in transverse sections of pollen tubes. The values on the images indicate the distance of the transverse sections from the tip of the pollen tubes. C, Kymograph analysis of the vesicle distributions in WT and *aip1-1* pollen tubes during their growth.

### Loss of function of *AtAIP1-1* reduces the dynamics of apical actin filaments in pollen tubes

Next, we examined the dynamics of actin filaments decorated with Lifeact-EGFP as described previously (Qu et al., 2013; Vidali et al., 2009). We specifically focused on examining actin filaments within the growth domain of pollen tubes. By kymograph analysis, we found that membrane-originated actin filaments occupied a wider region within *aip1-1* pollen tubes compared to WT pollen tubes (Figure 5A), and the overall length of membrane-originated actin filaments was significantly longer in *aip1-1* pollen tubes than in WT (Figure 5B). We next sought to examine the dynamics of individual actin filaments by tracing them and measuring the parameters associated with their dynamics (Figure 5C). The angles formed between the membrane-originated actin filaments and the growth axis of the pollen tubes were substantially increased in *aip1-1* pollen tubes compared to WT pollen tubes (Figure 5D), which is consistent with the observations shown in Figure 2F. In addition, we found that the average actin filament severing frequency decreased significantly in *aip1-1* pollen tubes compared to WT (Figure 5E). Actin monomer dissociation events also decreased substantially in *aip1-1* pollen tubes compared to WT (Figure 5E). Accordingly, we found that both maximal filament length and maximal filament lifetime increased significantly in *aip1-1* pollen tubes compared to WT (Figure 5E). However, there was no significant difference in actin filament elongation rate between *aip1-1* pollen tubes and WT pollen tubes (Figure 5E). Nonetheless, these data together suggest that the dynamics of actin filaments are reduced in *aip1-1* pollen tubes. This decrease in actin dynamics provides an explanation for why the rate of actin turnover is reduced in *aip1-1* pollen grains, as described above.

### AtAIP1-1 enhances ADF1-mediated actin depolymerization and severing

We next examined the activity of AtAIP1-1 in promoting ADF-mediated actin depolymerization. The well-characterized *Arabidopsis* ADF1 (Carlier et al., 1997) was taken as the representative plant actin-depolymerizing factor. We generated recombinant AtAIP1-1 protein (Figure 6A) and initially examined its effects on actin dynamics *in vitro* by high-speed F-actin cosedimentation experiments. We found that although AtAIP1-1 binds to actin filaments (Figure 6B and C), it does not affect the amount of actin in the pellet compared to actin alone (Figure 6D), which suggests that AtAIP1-1 does not have an obvious effect on actin assembly and disassembly *in vitro*. Next, we examined the effect of AtAIP1-1 on actin dynamics in the presence of ADF1. Consistent with a previous observation that ADF1 efficiently promotes actin depolymerization (Carlier et al., 1997), we found that ADF1 substantially enhances the amount of actin in the supernatant assayed with the high speed F-actin cosedimentation experiment (Figure 6E). Strikingly, the addition of AtAIP1-1 along with ADF1 substantially increases the amount of actin in the supernatant compared to ADF1 alone (Figure 6E). Furthermore, this effect of AtAIP1-1 on the ADF1-mediated increase in the amount of actin in the supernatant is dose-dependent (Figure 6F). These data suggest that AtAIP1-1 can enhance ADF1-mediated actin depolymerization. Given that ADF/cofilin also severs actin filaments, we used total internal reflection fluorescence microscopy (TIRFM) to investigate whether AtAIP1-1 can enhance ADF1-mediated severing of actin filaments. We found that the addition of

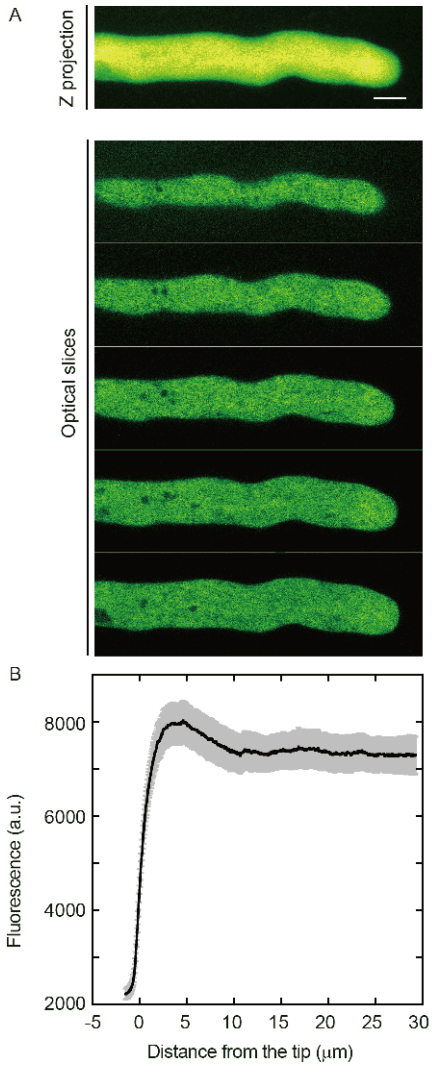


**Figure 4** AtAIP1-1 is distributed uniformly in pollen tubes. A, Images of AtAIP1-1-EGFP in a pollen tube. Both the projection image and optical sections are presented. Scale bar, 5 μm. B, Plot of the average fluorescence intensity of AtAIP1-1-EGFP in pollen tubes, starting from the tip and continuing along the growth axis. Data are presented as mean±SE (the black line is the mean and the shaded region shows the SE). More than 20 pollen tubes were measured.

AtAIP1-1 alone does not have an obvious effect on actin filaments when compared to the buffer control (Figure 6G(a and b)), whereas the addition of ADF1 alone caused fragmentation of actin filaments (Figure 6G(c)), which is consistent with the fact that ADF1 can sever actin filaments. Strikingly, actin filament fragmentation events increased substantially when AtAIP1-1 was added along with ADF1 (Figure 6G(d)). The effect of AtAIP1-1 on enhancing ADF1-mediated fragmentation of actin filaments was supported by measurements showing that the average actin filament severing frequency increases significantly in the presence of ADF1 and AtAIP1-1 compared to ADF1 alone (Figure 6H). These data suggest that AtAIP1-1 itself does not have an overt effect on actin assembly and disassembly, but it enhances ADF1-mediated actin depolymerization and actin filament severing *in vitro*.

## DISCUSSION

Here we demonstrate that AtAIP1-1 is involved in the regulation of the turnover and organization of apical actin filaments, which is crucial for tip-directed trafficking and accumulation of vesicles as well as normal pollen tube growth. Our *in vitro* and *in vivo* data suggest that AtAIP1-1 acts in concert with ADF to enhance the turnover of membrane-originated actin filaments within the growth domain of pollen tubes. This study, along with previous observations (Jiang et al., 2017), implicates AtAIP1-1/ADF as a regulatory module in the turnover and organization of membrane-originated actin filaments that are presumably nucleated by the membrane-anchored class I formins (Cheung et al., 2010; Lan et al., 2018). Consequently, this module facilitates the formation of the unique "apical actin structure" in pollen tubes (Qu et al., 2017). Our study thus substantially enhances our understanding of the cellular mechanisms underlying the regulation of the turnover and organization of membrane-originated actin filaments within the growth domain of pollen tubes.

Our *in vitro* biochemical data showed that AtAIP1-1 does not have an overt effect on actin assembly and disassembly, whereas it substantially enhances ADF1-mediated severing and depolymerization of actin filaments (Figure 6). This suggests that *Arabidopsis* AtAIP1-1 is biochemically similar to AIP1 homologues from other organisms (Jansen et al., 2015; Okada et al., 1999; Ono, 2001; Rodal et al., 1999; Shi et al., 2013). Accordingly, we found that actin filaments in *aip1-1* pollen grains are more resistant to treatment with latrunculin B than actin filaments in WT pollen grains (Figure S1D in Supporting Information), and actin filaments stained with fluorescent phalloidin are brighter overall in *aip1* pollen tubes than in WT pollen tubes (Figure 2A–C). The effect of loss of *AtAIP1-1* function on the actin cytoskeleton in pollen cells is similar to that reported in cells from other organisms or other cell types from the same organism (Augustine et al., 2011; Ketelaar et al., 2004; Konzok et al., 1999; Rodal et al., 1999; Shi et al., 2013). In addition, actin filaments became comparatively more disorganized in *aip1-1* pollen tubes (Figures 2A and 5C), which suggests that AtAIP1-1 is also involved in regulating the organization of actin filaments in pollen tubes. It was reported previously that ADF promotes the ordering of apical actin filaments by eliminating mis-aligned membrane-originated actin filaments in pollen tubes (Jiang et al., 2017). We think that AtAIP1-1 likely facilitates this function of ADF. In total, our *in vitro* and *in vivo* data suggest that the main function of AtAIP1-1 is to promote the turnover of membrane-originated

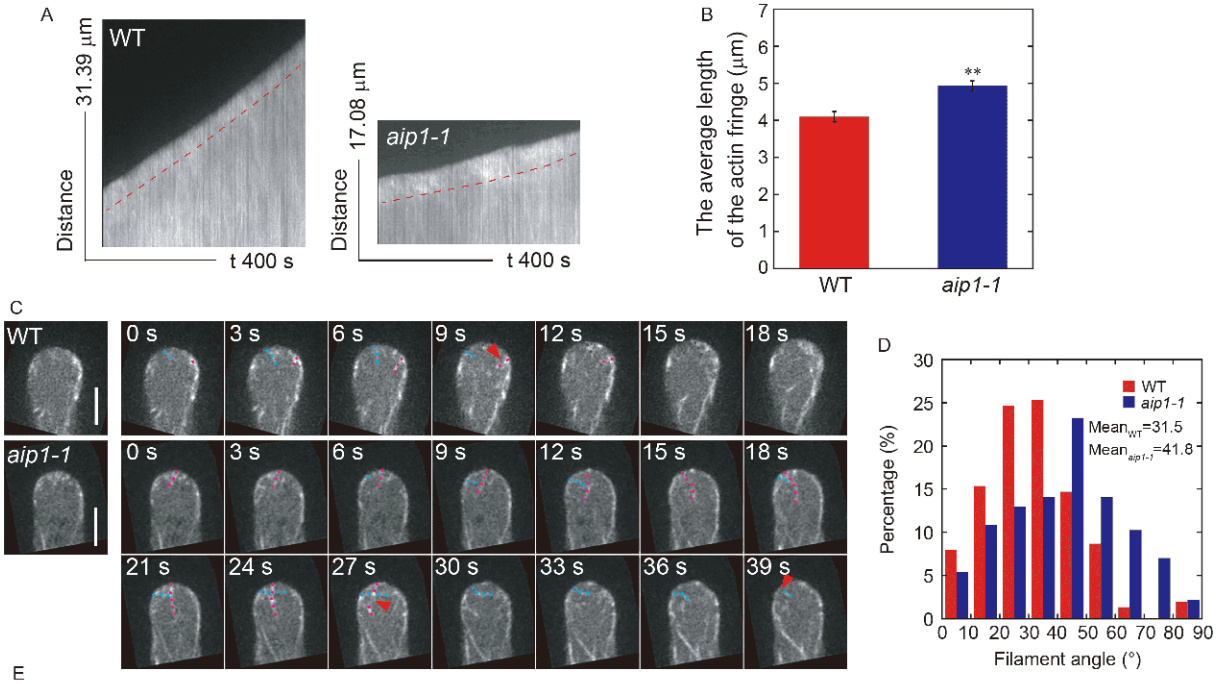


E

| Dynamic parameters | WT | *aip1-1* |
|---|---|---|
| Elongation rate, μm s $^{1}$ | 0.22±0.024(14) | 0.20±0.010(13) ND |
| Depolymerization rate, μm s $^{1}$ | 0.304±0.038(13) | 0.187±0.013(15)** |
| Severing frequency, breaks μm$^{-1}$ s$^{-1}$ | 0.0261±0.0049(15) | 0.0092±0.0017(13)* |
| Max filament length, μm | 2.54±0.138(27) | 4.08±0.328(27)** |
| Max filament life time, s | 20.9±1.76(21) | 32.1±2.22(26)** |

**Figure 5** Apical actin filaments become disorganized and are less dynamic in *aip1-1* pollen tubes. A, Kymograph analysis of apical actin filaments in WT and *aip1-1* pollen tubes during their growth. Red lines indicate the region occupied by apical actin filaments. B, Quantification of the average length of membrane-originated apical actin filaments in WT and *aip1-1* pollen tubes. More than 20 pollen tubes were measured. Data are presented as mean±SE, **, $P<0.01$ by Student's *t*-test. C, Actin filaments in the apical regions of WT and *aip1-1* pollen tubes revealed by decoration with Lifeact-GFP. Actin filaments are indicated by different colored dots. The red arrowheads indicate the actin filament severing events. Scale bar, 5 μm. D, Quantification of the angles formed between actin filaments and the growth axis of pollen tubes. More than 200 actin filaments were selected from more than 10 pollen tubes within the region 20 μm from the pollen tube tip. The values on the *Y*-axis represent the percentage of actin filaments within the ranges of angles shown on the *X*-axis. E, Statistical analysis of parameters of actin dynamics in WT and *aip1-1* pollen tubes. Values are presented as means±SD. The numbers of actin filaments analyzed are shown in in parentheses. *, $P<0.05$; **, $P<0.01$; ND, no significant difference. The statistical comparison between *aip1-1* and WT was performed by Student's *t*-test.

actin filaments and limit their lengths by acting in concert with ADF in pollen tubes, which consequently controls the construction of the unique "apical actin structure" within the growth domain of pollen tubes as proposed previously (Qu et al., 2017). Consequently, AtAIP1-1 controls the normal trafficking and accumulation of vesicles at the tip of pollen tube to drive its growth. Indeed, similar to the results in *adf10* mutant pollen tubes (Jiang et al., 2017), we found that the vesicle accumulation region became enlarged in *aip1-1* pollen tubes (Figure 3). This supports the previously proposed idea that apical actin filaments act as the physical barrier to spatially restrict the apically accumulated vesicles in the pollen tube (Kroeger et al., 2009). Our study therefore also provides insights into the functional relationship between actin filaments and vesicle transportation and accumulation within the growth domain of pollen tubes.

Our conclusion that the AtAIP1-1/ADF module mainly enhances the turnover of membrane-originated actin filaments and regulates their organization within the growth domain of pollen tubes differs from the previous notion that ADF promotes actin polymerization by fragmenting actin filaments to generate more free barbed ends for the addition of actin monomers (Lovy-Wheeler et al., 2005). The previous notion was mainly based on the hypothesis that actin filaments are generated locally at the subapex of pollen tubes (Lovy-Wheeler et al., 2005) and the observation that ADF (Chen et al., 2002) and AIP1 (Lovy-Wheeler et al., 2006) are concentrated at the subapex of the pollen tube. To reconcile the contradiction between the formation of prominent subapical actin structures and the concentration of ADF at the subapex of pollen tubes, the authors argued that ADF severs actin filaments to generate more barbed ends, thereby augmenting local actin polymerization at the subapex (Lovy-Wheeler et al., 2005). Indeed, ADF/cofilin is capable of

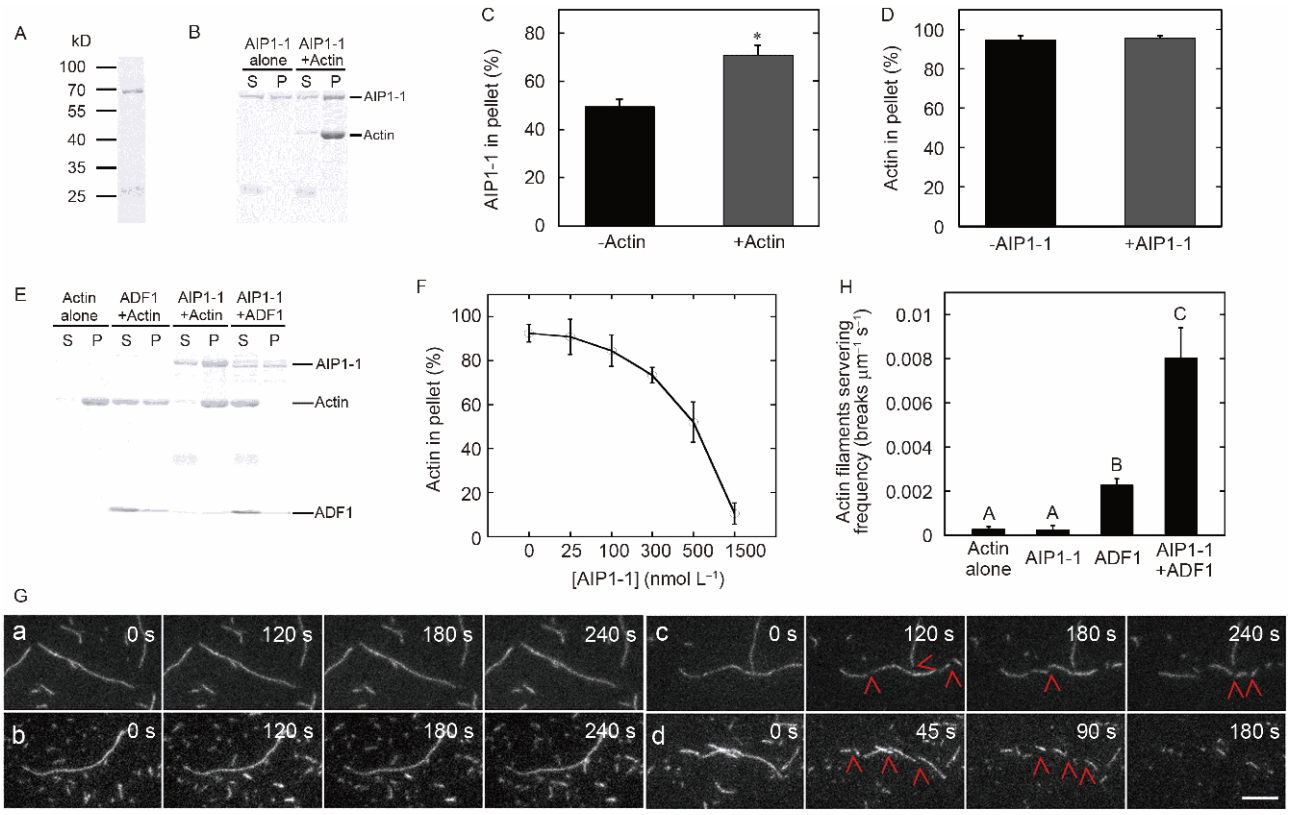


**Figure 6** AtAIP1-1 binds to actin filaments and enhances ADF1-mediated actin depolymerization in a dose-dependent manner. A, SDS-PAGE analysis of purified recombinant AtAIP1-1 protein. B, SDS-PAGE analysis of protein samples from the high-speed F-actin cosedimentation experiments. S, supernatant; P, pellet. [F-actin], 3 μmol $L^{-1}$; [AtAIP1-1], 1 μmol $L^{-1}$. C, Bar chart showing the amount of AtAIP1-1 in the pellet in the presence or absence of F-actin. Data are presented as mean±SE; *, $P<0.05$ by Student's *t*-test. D, Bar chart showing the amount of actin in the pellet in the presence or absence of AtAIP1-1. Data are presented as mean±SE. E, SDS-PAGE analysis of protein samples from F-actin cosedimentation analysis in the presence or absence of AtAIP1-1 and ADF1. S, supernatant; P, pellet. [F-actin], 3 μmol $L^{-1}$; [AtAIP1-1], 1 μmol $L^{-1}$; [ADF1], 10 μmol $L^{-1}$. F, Quantification of the amount of actin in the supernatant in the presence of 10 μmol $L^{-1}$ ADF1 and various amounts of AtAIP1-1. Data are presented as mean±SE. G, Time-lapse images of actin filaments in the absence or presence of ADF, AtAIP1-1 or ADF1+AtAIP1-1. Actin filaments were revealed by Oregon green. The red arrowheads indicate actin filament fragmentation events. Scale bar, 10 μm. H, Quantification of the average actin filament severing frequencies. Values represent mean±SE. Capital letters represent $P<0.01$ by Student's *t*-test.

promoting actin polymerization in mammalian cells (Ghosh et al., 2004). With the introduction of state-of-the-art live-cell imaging technology to trace the dynamics of actin filaments within growing pollen tubes, it is now clear that actin filaments are mainly generated from the membrane within the growth domain of pollen tubes (Cheung et al., 2010; Lan et al., 2018; Liu et al., 2015; Qu et al., 2013; Zhang et al., 2016). Given that membrane-originated actin filaments are nucleated by membrane-anchored formins within the growth domain of pollen tubes (Cheung et al., 2010; Lan et al., 2018), the ends of actin filaments growing toward the cytoplasm are pointed ends, which theoretically contain ADP-actin that is favored by ADF. We therefore propose a model in which AtAIP1-1/ADF trims membrane-originated actin filaments to maintain their lengths and construct the unique apical actin structure in the pollen tube. In summary, our study provides significant insights into the cellular mechanisms underlying the regulation of the construction of the apical actin structure in the pollen tube.

## MATERIALS AND METHODS

### Plant materials and growth conditions

The *AtAIP1-1* T-DNA insertion line CSHL_GT8956 was obtained from Nottingham *Arabidopsis* Stock Centre (NASC). Since CSHL_GT8956 is in the Landsberg background, it was backcrossed three times with the *Arabidopsis* Columbia-0 (Col-0) ecotype. After segregation, the wild type (WT) siblings were used as the WT plants in this study. *Arabidopsis* plants were grown in a culture room at 22°C under a 16-h light/8-h dark photoperiod.

### Plasmid construction

In order to determine the intracellular localization of AtAIP1-1, a construct containing a carboxyl (C)-terminal EGFP fusion of AtAIP1-1 was generated with expression driven by the native *AtAIP1-1* promoter. The PCR fragments were amplified with proAIP1-1-F-USCA/proAIP1-1-R-

USCA, gAIP1-1-F-USCA-C/gAIP1-1-R-USCA-C and EGFP-F-USCA-C/EGFP-R-USCA-C (Table S1 in Supporting Information) using *Arabidopsis* genomic DNA as the template and moved into pCambia1301 with the seamless ligation method to generate pCambia1301-AtAIP1-1-EGFP. To generate recombinant AtAIP1-1 protein, the coding region sequence of *AtAIP1-1* was amplified with primer pair AIP1-1F (*Nde* I)/AIP1-1R (*Sal* I) (Table S1 in Supporting Information), and the error-free PCR product was moved into pET28a restricted with *Nde* I/*Sal* I to generate pET28a-AtAIP1-1 plasmid.

### Complementation and visualization of the intracellular localization of AtAIP1-1 in pollen tubes

The pCambia1301-AtAIP1-1-EGFP plasmid was introduced into *Agrobacterium tumefaciens* strain GV3101 and transformed into *aip1-1* plants via the floral dip method (Clough and Bent, 1998). The transgenic plants were designated as *AIP1-1p:AIP1-1-EGFP;aip1-1*. Pollen grains derived from the T3 homozygous transgenic plants were used to analyze the intracellular localization of AtAIP1-1 in pollen tubes. The images of AIP1-1-EGFP in *Arabidopsis* pollen tubes were obtained with an Olympus FV1200 laser scanning confocal microscope excited under a 488-nm argon laser with the emission wavelength set at 500–550 nm. The z-series images were collected with the z-step size set at 0.5 μm. The projection of z-series images was performed with ImageJ software (http://rsbweb.nih.gov/ij/; version 1.48g) and the fluorescence intensity of AIP1-1-EGFP in pollen tubes was measured with the same software.

### RT-PCR

RT-PCR was performed to determine the transcript levels of *AtAIP1-1* in pollen derived from WT, *aip1-1* and the complementation lines. Total RNA was isolated from pollen using Trizol reagent (Invitrogen) and was reverse transcribed using MMLV reverse transcriptase (Promega) according to the manufacturer's instructions. To amplify full-length *AtAIP1-1* transcripts, semi-quantitative RT-PCR analysis was performed with primer pair AIP1-1F (*Nde* I)/AIP1-1R(*Sal* I) (Table S1 in Supporting Information). The amount of *AtAIP1-1* transcripts was also determined by the quantitative RT-PCR analysis with the primer pair qAtAIP1-1F/qAtAIP1-1R (Table S1 in Supporting Information). *eIF4A* was amplified as an internal control with primer pair $eIF4A_{FOR}$/$eIF4A_{REV}$ (Table S1 in Supporting Information). The $2^{-\Delta\Delta C_t}$ method (Livak and Schmittgen, 2001) was used to quantify the qRT-PCR results. 2×RealStar Power SYBR Mixture (GeneStar) was used for the amplification.

### *In vitro Arabidopsis* pollen germination and pollen tube growth and measurements

*Arabidopsis* pollen germination *in vitro* was performed essentially according to a previously published method (Wu et al., 2010; Yu et al., 2018). Briefly, freshly opened *Arabidopsis* flowers were collected and then touched onto the surface of pollen germination medium (GM: 1 mmol $L^{-1}$ $CaCl_2$, 1 mmol $L^{-1}$ $Ca(NO_3)_2$, 1 mmol $L^{-1}$ $MgSO_4$, 0.01% (w/v) $H_3BO_3$, and 18% (w/v) sucrose, pH 6.9–7.0 solidified with the addition of 0.8% (w/v) agar). Pollen germination was performed at 28°C under moist conditions. The determination of pollen germination percentage and pollen tube growth rates was performed exactly according to the previously published method (Wu et al., 2010). To determine the effect of latrunculin B (LatB) on pollen germination, the required amount of LatB was included into the GM before the solidification of the GM. The experiments were repeated at least three times.

### Actin staining with Alexa-488-phalloidin in fixed pollen grains and pollen tubes, and quantification

Staining of actin filaments in fixed pollen grains and pollen tubes was performed roughly according to a previously published method (Wu et al., 2010). Briefly, after being cultured on the surface of solid pollen GM for 1 h, they were subjected to treatment with 300 μmol $L^{-1}$ *m*-maleimidobenzoyl-*N*-hydroxysuccinimide ester in liquid GM for 1 h. After treatment with 0.05% NP-40 in liquid GM for 10 min, pollen grains and pollen tubes were washed with TBSS (50 mmol $L^{-1}$ Tris-HCl, pH 7.5, 200 mmol $L^{-1}$ NaCl, and 400 mmol $L^{-1}$ sucrose) three times. The treated samples were subsequently incubated with 200 nmol $L^{-1}$ Alexa-488 phalloidin overnight at 4°C. The images were collected using an Olympus FV1200 laser scanning confocal microscope excited with a 488-nm argon laser with the emission wavelengths set at 500–550 nm. Transverse sections of pollen tubes were generated with ImageJ and three-dimensional graphs of the intensities of each pixel in the transverse sections were generated by the built-in "Surface plot" tool in ImageJ. A pseudo Rainbow RGB color was applied to the surface plots to assess the intensities by colors ranging from dark blue to bright red. The fluorescence intensity of Alexa-488 phalloidin-staining was measured to reflect the amount of actin filaments as described previously (Ye et al., 2009). To determine the effects of LatB treatment on the actin cytoskeleton in pollen grains, 150 nmol $L^{-1}$ LatB was included in the pollen GM and incubated for 30 min.

### Visualization and quantification of actin filament dynamics in pollen tubes

Actin filaments in living pollen tubes were decorated with

Lifeact-EGFP as described previously (Qu et al., 2013; Vidali et al., 2009). The Lifeact-EGFP marker was introduced into *aip1-1* mutant pollen tubes by crossing WT plants expressing *Lat52:Lifeact-EGFP* with *aip1-1* mutant plants. Pollen derived from the *aip1-1* mutant plants and sibling WT plants expressing *Lat52:Lifeact-EGFP* were used to visualize actin dynamics in pollen tubes after the average length of pollen tubes reached about 150 μm. Pollen tubes were observed under a spinning disk confocal microscope equipped with a 100× oil objective. The time-lapse images were acquired with an Andor iXon3 DU888 EMCCD camera at its fastest collecting rate and the z-step size was set at 0.5 μm. The collected images were processed with ImageJ software and the parameters of the dynamics of actin filaments, such as elongation rates, depolymerization rates, maximal filament lifetime, maximal filament length and severing frequency, were measured as described previously (Staiger et al., 2009). Specifically, the severing frequency was determined by counting all severing events from the filament at its longest length to its disappearance. The elongation and depolymerization rates of actin filaments were calculated as the changes of length versus the time intervals. The kymograph analysis was performed to analyze the dynamics of membrane-originated apical actin filaments as previously described (Qu et al., 2017).

### Visualization of the distribution and dynamics of YFP-RabA4b in living pollen tubes

YFP-RabA4b was used to label transport vesicles in pollen tubes as described previously (Zhang et al., 2010b). To introduce YFP-RabA4b into the *aip1-1* mutant, *aip1-1* mutant plants were crossed with WT plants expressing *LAT52:YFP-RabA4b*. After segregation, the WT sibling plants and *aip1-1* mutant plants harboring *LAT52:YFP-RabA4b* were used for subsequent analysis and comparison. The samples were observed under a spinning disk confocal microscope (Yokogawa CSUX1FW) and the time-lapse images were acquired with an Andor iXon3 DU888 EMCCD camera at 2 s time-intervals and a step size of 0.7 μm. The distribution of the fluorescence intensity of YFP-RabA4b in transverse sections of pollen tubes was analyzed with the built-in "Surface plot" tool in ImageJ. To analyze the turnover rate of vesicles, fluorescence recovery after photobleaching (FRAP) experiments were performed as described previously (Chang and Huang, 2015). The selected region was photobleached for 4 s with laser power at 25% for the 405 nm laser and 100% for the 488 nm laser, and the time-lapse images after photobleaching were collected at 2 s intervals. The statistical analysis of recovery time was performed as described previously (Chang and Huang, 2015). Experiments were repeated at last 10 times and the values of YFP-RabA4b fluorescence were averaged and used for subsequent exponential curve fitting.

### Protein production

To generate recombinant AtAIP1-1 protein, pET28a-AtAIP1-1 was introduced into *E. coli*, BL21 DE3 strain. After the $A_{600}$ of bacterial solution reached about 1.0, protein expression was induced by the addition of 0.4 mmol $L^{-1}$ isopropyl β-D-1-thiogalactopyranoside for 4 h at 37°C. The bacteria were collected by centrifugation and resuspended in 1× Binding Buffer (25 mmol $L^{-1}$ Tris-HCl, pH 7.9, 250 mmol $L^{-1}$ KCl, 5 mmol $L^{-1}$ imidazole, and 2 mmol $L^{-1}$ mercaptoethanol), and the 6His-AIP1-1 protein was purified with nickel sepharose according to the manufacturer's instructions. The purified proteins were dialyzed against G buffer (5 mmol $L^{-1}$ Tris-HCl, pH 8.0, 0.2 mmol $L^{-1}$ ATP, 0.1 mmol $L^{-1}$ $CaCl_2$, and 0.5 mmol $L^{-1}$ DTT) and aliquoted, then flash frozen in liquid nitrogen and stored in a –80°C freezer. ADF1 was purified according to Carlier et al. (1997). Purification of actin from rabbit skeletal muscle was carried out as described previously (Pollard, 1984; Spudich and Watt, 1971) and labeling of actin with Oregon-green was performed according to the published method (Amann and Pollard, 2001a).

### High-speed F-actin cosedimentation assay

The high-speed F-actin cosedimentation assay was performed as described previously (Kovar et al., 2000). Briefly, preassembled actin filaments (3 μmol $L^{-1}$) were incubated at room temperature for 1 h with 10 μmol $L^{-1}$ ADF1 or 10 μmol $L^{-1}$ ADF1 in the presence or absence of various concentrations of AtAIP1-1, or with AtAIP1-1 alone. The reaction mixtures were subjected to centrifugation for 30 min under 100,000×*g*. The pellet and supernatant fractions were separated by 15% SDS-PAGE, and the amount of actin in supernatant and pellet fractions was measured by densitometry.

### Direct visualization of actin filament severing by total internal reflection fluorescence microscopy (TIRFM)

The dynamics of individual actin filaments on a cover-glass in a flow chamber were visualized with TIRFM as previously described (Amann and Pollard, 2001b). The flow chambers were prepared as described previously (Jiang and Huang, 2017; Kovar and Pollard, 2004). After injection of preassembled 50%-labeled Oregon-Green actin filaments at 1 μmol $L^{-1}$ into the flow chamber, AtAIP1-1, ADF, or ADF plus AtAIP1-1 in 1× TIRFM Buffer (10 mmol $L^{-1}$ imidazole, pH 7.0, 50 mmol $L^{-1}$ KCl, 1 mmol $L^{-1}$ $MgCl_2$, 1 mmol $L^{-1}$ EGTA, 50 mmol $L^{-1}$ dithiothreitol, 0.2 mmol $L^{-1}$ ATP, 50 μmol $L^{-1}$ $CaCl_2$, 15 mmol $L^{-1}$ glucose, 20 μg $mL^{-1}$ cata-

lase, 100 μg $mL^{-1}$ glucose oxidase and 0.5% methylcellulose) were injected into the flow chamber. The time-lapse images were acquired at 3 s intervals by the Andor iXon3 DU888 EMCCD camera with microManager software (www.micro-manager.org). Actin filaments of length >10 μm were selected for the quantification of actin filament severing frequency (defined as the number of breaks per filament length per time; breaks $\mu m^{-1} s^{-1}$) as described previously (Bao et al., 2012; Khurana et al., 2010). To determine the dissociation rate (subunits $s^{-1}$) of actin monomers, the length of actin filaments (μm) was converted into subunits by assuming that there are 334 subunits per μm length of actin filament.

**Compliance and ethics** *The author(s) declare that they have no conflict of interest.*

**Acknowledgements** *We thank Yan Zhang (Shandong Agricultural University) for providing the transgenic lines expressing Lat52:YFP-RabA4b. This work was supported by a grant from the National Natural Science Foundation of China (31671390) and funding from the Tsinghua-Peking Joint Center for Life Sciences.*

## References

Allwood, E.G., Anthony, R.G., Smertenko, A.P., Reichelt, S., Drobak, B. K., Doonan, J.H., Weeds, A.G., and Hussey, P.J. (2002). Regulation of the pollen-specific actin-depolymerizing factor LlADF1. Plant Cell 14, 2915–2927.

Amann, K.J., and Pollard, T.D. (2001a). The Arp2/3 complex nucleates actin filament branches from the sides of pre-existing filaments. Nat Cell Biol 3, 306–310.

Amann, K.J., and Pollard, T.D. (2001b). Direct real-time observation of actin filament branching mediated by Arp2/3 complex using total internal reflection fluorescence microscopy. Proc Natl Acad Sci USA 98, 15009–15013.

Amberg, D.C., Basart, E., and Botstein, D. (1995). Defining protein interactions with yeast actin *in vivo*. Nat Struct Mol Biol 2, 28–35.

Augustine, R.C., Pattavina, K.A., Tüzel, E., Vidali, L., and Bezanilla, M. (2011). Actin interacting protein1 and actin depolymerizing factor drive rapid actin dynamics in *Physcomitrella patens*. Plant Cell 23, 3696–3710.

Bao, C., Wang, J., Zhang, R., Zhang, B., Zhang, H., Zhou, Y., and Huang, S. (2012). *Arabidopsis* VILLIN2 and VILLIN3 act redundantly in sclerenchyma development via bundling of actin filaments. Plant J 71, 962–975.

Bou Daher, F., van Oostende, C., and Geitmann, A. (2011). Spatial and temporal expression of actin depolymerizing factors ADF7 and ADF10 during male gametophyte development in *Arabidopsis thaliana*. Plant Cell Physiol 52, 1177–1192.

Carlier, M.F., Laurent, V., Santolini, J., Melki, R., Didry, D., Xia, G.X., Hong, Y., Chua, N.H., and Pantaloni, D. (1997). Actin depolymerizing factor (ADF/cofilin) enhances the rate of filament turnover: implication in actin-based motility. J Cell Biol 136, 1307–1322.

Chang, M., and Huang, S. (2015). *Arabidopsis* ACT11 modifies actin turnover to promote pollen germination and maintain the normal rate of tube growth. Plant J 83, 515–527.

Chen, C.Y., Wong, E.I., Vidali, L., Estavillo, A., Hepler, P.K., Wu, H., and Cheung, A.Y. (2002). The regulation of actin organization by actin-depolymerizing factor in elongating pollen tubes. Plant Cell 14, 2175–2190.

Chen, N., Qu, X., Wu, Y., and Huang, S. (2009). Regulation of actin dynamics in pollen tubes: control of actin polymer level. J Integrat Plant Biol 51, 740–750.

Cheung, A.Y., Niroomand, S., Zou, Y., and Wu, H.M. (2010). A transmembrane formin nucleates subapical actin assembly and controls tip-focused growth in pollen tubes. Proc Natl Acad Sci USA 107, 16390–16395.

Cheung, A.Y., and Wu, H.M. (2008). Structural and signaling networks for the polar cell growth machinery in pollen tubes. Annu Rev Plant Biol 59, 547–572.

Clough, S.J., and Bent, A.F. (1998). Floral dip: a simplified method for Agrobacterium-mediated transformation of *Arabidopsis thaliana*. Plant J 16, 735–743.

Daher, F.B., and Geitmann, A. (2012). Actin depolymerizing factors ADF7 and ADF10 play distinct roles during pollen development and pollen tube growth. Plant Signal Behav 7, 879–881.

Fu, Y. (2015). The cytoskeleton in the pollen tube. Curr Opin Plant Biol 28, 111–119.

Ghosh, M., Song, X., Mouneimne, G., Sidani, M., Lawrence, D.S., and Condeelis, J.S. (2004). Cofilin promotes actin polymerization and defines the direction of cell motility. Science 304, 743–746.

Gibbon, B.C., Kovar, D.R., and Staiger, C.J. (1999). Latrunculin B has different effects on pollen germination and tube growth. Plant Cell 11, 2349–2364.

Jansen, S., Collins, A., Chin, S.M., Ydenberg, C.A., Gelles, J., and Goode, B.L. (2015). Single-molecule imaging of a three-component ordered actin disassembly mechanism. Nat Commun 6, 7202.

Jiang, Y., and Huang, S. (2017). Direct visualization and quantification of the actin nucleation and elongation events *in vitro* by TIRF microscopy. Bio Protoc 7.

Jiang, Y., Wang, J., Xie, Y., Chen, N., and Huang, S. (2017). ADF10 shapes the overall organization of apical actin filaments by promoting their turnover and ordering in pollen tubes. J Cell Sci 130, 3988–4001.

Ketelaar, T., Allwood, E.G., Anthony, R., Voigt, B., Menzel, D., and Hussey, P.J. (2004). The actin-interacting protein AIP1 is essential for actin organization and plant development. Curr Biol 14, 145–149.

Khurana, P., Henty, J.L., Huang, S., Staiger, A.M., Blanchoin, L., and Staiger, C.J. (2010). *Arabidopsis* VILLIN1 and VILLIN3 have overlapping and distinct activities in actin bundle formation and turnover. Plant Cell 22, 2727–2748.

Kiefer, C.S., Claes, A.R., Nzayisenga, J.C., Pietra, S., Stanislas, T., Hüser, A., Ikeda, Y., and Grebe, M. (2015). *Arabidopsis* AIP1-2 restricted by WER-mediated patterning modulates planar polarity. Development 142, 151–161.

Konzok, A., Weber, I., Simmeth, E., Hacker, U., Maniak, M., and Müller-Taubenberger, A. (1999). Daip1, a *Dictyostelium* homologue of the yeast actin-interacting protein 1, is involved in endocytosis, cytokinesis, and motility. J Cell Biol 146, 453–464.

Kovar, D.R., and Pollard, T.D. (2004). Insertional assembly of actin filament barbed ends in association with formins produces piconewton forces. Proc Natl Acad Sci USA 101, 14725–14730.

Kovar, D.R., Staiger, C.J., Weaver, E.A., and McCurdy, D.W. (2000). AtFim1 is an actin filament crosslinking protein from *Arabidopsis thaliana*. Plant J 24, 625–636.

Kroeger, J.H., Daher, F.B., Grant, M., and Geitmann, A. (2009). Microfilament orientation constrains vesicle flow and spatial distribution in growing pollen tubes. Biophys J 97, 1822–1831.

Lan, Y., Liu, X., Fu, Y., and Huang, S. (2018). *Arabidopsis* class I formins control membrane-originated actin polymerization at pollen tube tips. PLoS Genet 14, e1007789.

Liu, X., Qu, X., Jiang, Y., Chang, M., Zhang, R., Wu, Y., Fu, Y., and Huang, S. (2015). Profilin regulates apical actin polymerization to control polarized pollen tube growth. Mol Plant 8, 1694–1709.

Livak, K.J., and Schmittgen, T.D. (2001). Analysis of relative gene expression data using real-time quantitative PCR and the $2^{-\Delta\Delta C_T}$ method. Methods 25, 402–408.

Lovy-Wheeler, A., Kunkel, J.G., Allwood, E.G., Hussey, P.J., and Hepler, P.K. (2006). Oscillatory increases in alkalinity anticipate growth and

may regulate actin dynamics in pollen tubes of lily. Plant Cell 18, 2182–2193.
Lovy-Wheeler, A., Wilsen, K.L., Baskin, T.I., and Hepler, P.K. (2005). Enhanced fixation reveals the apical cortical fringe of actin filaments as a consistent feature of the pollen tube. Planta 221, 95–104.
Okada, K., Obinata, T., and Abe, H. (1999). XAIP1: a *Xenopus* homologue of yeast actin interacting protein 1 (AIP1), which induces disassembly of actin filaments cooperatively with ADF/cofilin family proteins. J Cell Sci 112, 1553–1565.
Ono, S. (2001). The *Caenorhabditis elegans unc-78* gene encodes a homologue of actin-interacting protein 1 required for organized assembly of muscle actin filaments. J Cell Biol 152, 1313–1320.
Pollard, T.D. (1984). Polymerization of ADP-actin. J Cell Biol 99, 769–777.
Qu, X., Jiang, Y., Chang, M., Liu, X., Zhang, R., and Huang, S. (2015). Organization and regulation of the actin cytoskeleton in the pollen tube. Front Plant Sci 5, 786.
Qu, X., Zhang, H., Xie, Y., Wang, J., Chen, N., and Huang, S. (2013). *Arabidopsis* villins promote actin turnover at pollen tube tips and facilitate the construction of actin collars. Plant Cell 25, 1803–1817.
Qu, X., Zhang, R., Zhang, M., Diao, M., Xue, Y., and Huang, S. (2017). Organizational innovation of apical actin filaments drives rapid pollen tube growth and turning. Mol Plant 10, 930–947.
Ren, H., and Xiang, Y. (2007). The function of actin-binding proteins in pollen tube growth. Protoplasma 230, 171–182.
Rodal, A.A., Tetreault, J.W., Lappalainen, P., Drubin, D.G., and Amberg, D.C. (1999). Aip1p interacts with cofilin to disassemble actin filaments. J Cell Biol 145, 1251–1264.
Shi, M., Xie, Y., Zheng, Y., Wang, J., Su, Y., Yang, Q., and Huang, S. (2013). *Oryza sativa* actin-interacting protein 1 is required for rice growth by promoting actin turnover. Plant J 73, 747–760.
Smertenko, A.P., Allwood, E.G., Khan, S., Jiang, C.J., Maciver, S.K., Weeds, A.G., and Hussey, P.J. (2001). Interaction of pollen-specific actin-depolymerizing factor with actin. Plant J 25, 203–212.
Spudich, J.A., and Watt, S. (1971). The regulation of rabbit skeletal muscle contraction. I. Biochemical studies of the interaction of the tropomyosin-troponin complex with actin and the proteolytic fragments of myosin. J Biol Chem 246, 4866–4871.
Staiger, C.J., Poulter, N.S., Henty, J.L., Franklin-Tong, V.E., and Blanchoin, L. (2010). Regulation of actin dynamics by actin-binding proteins in pollen. J Exp Bot 61, 1969–1986.
Staiger, C.J., Sheahan, M.B., Khurana, P., Wang, X., McCurdy, D.W., and Blanchoin, L. (2009). Actin filament dynamics are dominated by rapid growth and severing activity in the *Arabidopsis* cortical array. J Cell Biol 184, 269–280.
Vidali, L., McKenna, S.T., and Hepler, P.K. (2001). Actin polymerization is essential for pollen tube growth. Mol Bio Cell 12, 2534–2545.
Vidali, L., Rounds, C.M., Hepler, P.K., and Bezanilla, M. (2009). Lifeact-mEGFP reveals a dynamic apical F-actin network in tip growing plant cells. PLoS ONE 4, e5744.
Wu, Y., Yan, J., Zhang, R., Qu, X., Ren, S., Chen, N., and Huang, S. (2010). *Arabidopsis* FIMBRIN5, an actin bundling factor, is required for pollen germination and pollen tube growth. Plant Cell 22, 3745–3763.
Ye, J., Zheng, Y., Yan, A., Chen, N., Wang, Z., Huang, S., and Yang, Z. (2009). *Arabidopsis* Formin3 directs the formation of actin cables and polarized growth in pollen tubes. Plant Cell 21, 3868–3884.
Yu, Y., Song, J., Tian, X., Zhang, H., Li, L., and Zhu, H. (2018). *Arabidopsis* PRK6 interacts specifically with AtRopGEF8/12 and induces depolarized growth of pollen tubes when overexpressed. Sci China Life Sci 61, 100–112.
Zhang, H., Qu, X., Bao, C., Khurana, P., Wang, Q., Xie, Y., Zheng, Y., Chen, N., Blanchoin, L., Staiger, C.J., et al. (2010a). *Arabidopsis* VILLIN5, an actin filament bundling and severing protein, is necessary for normal pollen tube growth. Plant Cell 22, 2749–2767.
Zhang, M., Zhang, R., Qu, X., and Huang, S. (2016). *Arabidopsis* FIM5 decorates apical actin filaments and regulates their organization in the pollen tube. J Exp Bot 67, 3407–3417.
Zhang, Y., He, J., Lee, D., and McCormick, S. (2010b). Interdependence of endomembrane trafficking and actin dynamics during polarized growth of *Arabidopsis* pollen tubes. Plant Physiol 152, 2200–2210.
Zheng, Y., Xie, Y., Jiang, Y., Qu, X., and Huang, S. (2013). *Arabidopsis* actin-depolymerizing factor7 severs actin filaments and regulates actin cable turnover to promote normal pollen tube growth. Plant Cell 25, 3405–3423.
Zhu, J., Nan, Q., Qin, T., Qian, D., Mao, T., Yuan, S., Wu, X., Niu, Y., Bai, Q., An, L., et al. (2017). Higher-ordered actin structures remodeled by *Arabidopsis* ACTIN-DEPOLYMERIZING FACTOR5 are important for pollen germination and pollen tube growth. Mol Plant 10, 1065–1081.

## SUPPORTING INFORMATION

**Figure S1** AtAIP1-1-eGFP is functional.

**Figure S2** The velocity of tip-directed vesicle transport is reduced in *aip1-1* pollen tubes.

**Table S1** Primers used in this paper

The supporting information is available online at http://life.scichina.com and https://link.springer.com. The supporting materials are published as submitted, without typesetting or editing. The responsibility for scientific accuracy and content remains entirely with the authors.